

Article

Distribution of Trace Elements in K-Feldspar with Implications for Tracing Ore-Forming Processes in Pegmatites: Examples from the World-Class Kolmozero Lithium Deposit, NW Russia

Lyudmila Morozova ^{1,2,*}, Dmitry Zozulya ¹ , Ekaterina Selivanova ¹ , Pavel Serov ¹  and Aya Bazai ¹

¹ Geological Institute of the Kola Science Centre of the Russian Academy of Sciences, 14 Fersman St., 184209 Apatity, Russia

² All-Russian Scientific-Research Institute of Mineral Resources Named after N.M. Fedorovsky, 31 Staromonetny Ln, 119017 Moscow, Russia

* Correspondence: morozova@geoksc.apatity.ru

Abstract: This study utilizes LA-ICP-MS-determined minor and trace element contents of megacrystic blocky K-feldspar to reveal the chemical variability and fractionation degree of albite-spodumene and barren feldspar pegmatites of the Kolmozero lithium deposit in the Kola region, Russia. K-feldspar from albite-spodumene pegmatite is represented by two generations: early microcline-I and late microcline-II. Rb, Cs, Li, and Tl are the most typical impurity elements in K-feldspar that replace K in its crystal lattice. Microcline-II differs from microcline-I: (i) relatively high contents of Rb (6520 and 4490 ppm, respectively), Cs (146 and 91 ppm), and Li (86 and 68 ppm), Tl (34 and 28 ppm); and (ii) low contents of Ba (13 and 29 ppm), Sr (8 and 24 ppm), and Pb (14 and 26 ppm). K-feldspar from feldspar pegmatites of the Kolmozero pegmatite field differs from those in the Kolmozero Li deposit in (i) low contents of Rb, Cs, Li, Tl, and an orthoclase component; and (ii) high contents of Sr, Ba, Pb, and an albite component. K/Sr, K/Ba, Rb/Ba, and Rb/Sr element ratios increase, while K/Rb, K/Cs, K/Tl, and K/Li element ratios decrease in K-feldspar, from feldspar pegmatites to albite-spodumene pegmatites. These trends reflect different fractionation degrees of pegmatite evolution. The implications of the detected trace element variations in K-feldspar are discussed in respect of tracing the rare element enrichments in pegmatite systems. A model is proposed for the formation of the Kolmozero pegmatites by differentiation from a hypothetical parental granite, rather than by anatexis of the host rock.

Keywords: K-feldspar; LA-ICP-MS; Kolmozero lithium deposit; trace elements; Russian Arctic; Fennoscandian Shield



Citation: Morozova, L.; Zozulya, D.; Selivanova, E.; Serov, P.; Bazai, A. Distribution of Trace Elements in K-Feldspar with Implications for Tracing Ore-Forming Processes in Pegmatites: Examples from the World-Class Kolmozero Lithium Deposit, NW Russia. *Minerals* **2022**, *12*, 1448. <https://doi.org/10.3390/min12111448>

Academic Editors: Nathan Fox and Rick Valenta

Received: 30 August 2022

Accepted: 14 November 2022

Published: 16 November 2022

Publisher's Note: MDPI stays neutral with regard to jurisdictional claims in published maps and institutional affiliations.



Copyright: © 2022 by the authors. Licensee MDPI, Basel, Switzerland. This article is an open access article distributed under the terms and conditions of the Creative Commons Attribution (CC BY) license (<https://creativecommons.org/licenses/by/4.0/>).

1. Introduction

Rare-metal (Li, Cs, Ta, Nb)-bearing peralkaline and peraluminous pegmatites represent the world's largest hard rock resource of lithium [1,2]. Numerous studies have been carried out on the mineral chemistry of K-feldspar in order to elucidate the conditions of pegmatite formation and its role in controlling the rare metal content of pegmatites [3–12]. The minor and trace element chemistry of K-feldspar, one of the most common minerals in these pegmatites, has been utilized to better understand genetic aspects of pegmatite formation, including the degree of fractionation of the magma and the relationships among different pegmatites within a pegmatite field, and to assess the economic potential of pegmatites for rare metal mineralization. The genesis of rare-metal pegmatites is, however, still debated (e.g., [9,13]).

This study provides the first data on minor and trace elements in K-feldspar from albite-spodumene pegmatites of the Kolmozero Li deposit in the Kola region, north-eastern Fennoscandian Shield. Indicative ratios of trace elements established for the Kolmozero K-feldspar have practical application for assessing the economic potential of pegmatites in

the Kola region and contribute to a better understanding of the genetic environment of the formation of the pegmatite systems. Mining of the Kolmozero deposit will commence in 2023–2024.

2. Geological Setting

2.1. Regional Geology

Albite-spodumene pegmatites comprising the Kolmozero Li deposit are part of the Kolmozero pegmatite field situated at the lithotectonic boundary separating the Archaean Kola and Murmansk provinces of the Fennoscandian Shield (Figure 1). Based on mineralogical and structural characteristics, albite-spodumene, muscovite-feldspar, and feldspar pegmatites have been distinguished in the Kolmozero pegmatite field. The albite-spodumene pegmatites contain Be-Ta-Nb-Li mineralization and are considered to represent the Kolmozero Li deposit, the muscovite-feldspar pegmatites, which are mineralized in Be-Nb-Ta, and the feldspar pegmatites, which only show Be-enrichments [14,15].

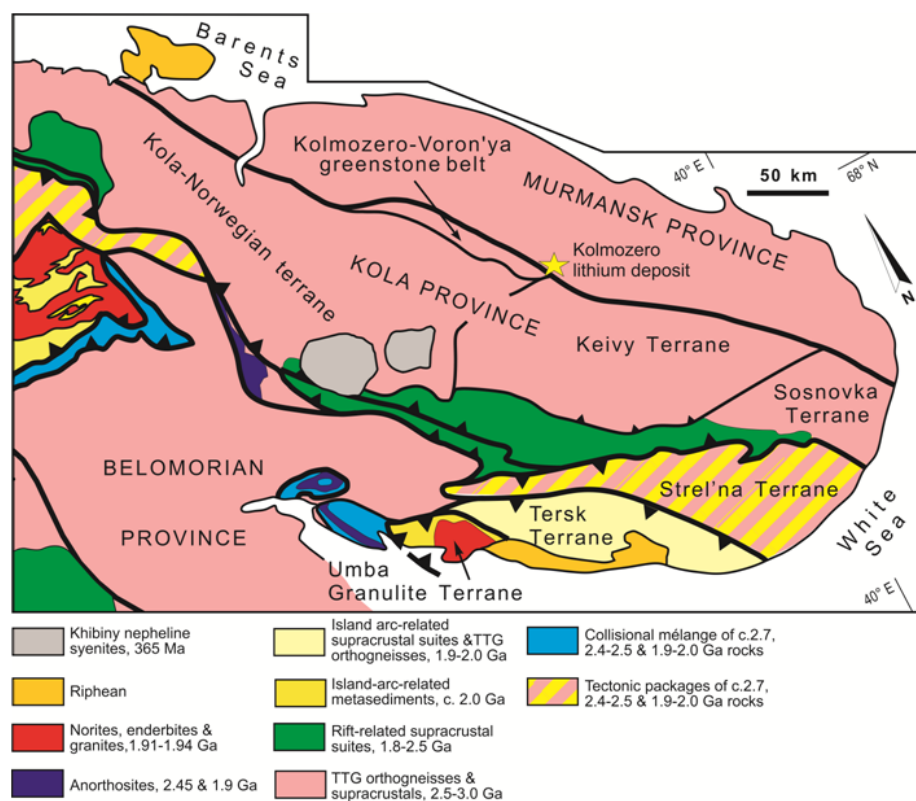


Figure 1. Tectonic provinces of the north-eastern Fennoscandian Shield. Modified after Daly et al. [16]. The asterisk marks the area shown in Figure 2.

The Murmansk province (2.68–2.94 Ga; [17]) is mainly composed of Late Mesoproterozoic and Neoproterozoic tonalite-trondhjemite gneisses, granites, charnockites, and enderbites with relics of supracrustal rocks, which were mostly subject to high-temperature metamorphism to amphibolite facies with granulite facies mineral assemblages being rare. Mineral assemblages of granulite facies are rare [18,19]. The Kola province comprises the Kolmozero-Voron'ya greenstone belt, and the Kola-Norwegian and Keivy terranes. The Late Mesoproterozoic Kolmozero-Voron'ya greenstone belt (2.79–2.92 Ga; [20]) is composed of metabasalts, metakomatiites, and metasedimentary rocks. The greenstone rocks underwent amphibolite-facies metamorphism. The Kola-Norwegian and Keivy terranes consist of tonalite-trondhjemite-granodiorite gneisses, enderbites, charnockites, amphibolites and metasediments [20].

The continental crust of the Murmansk and Kola provinces in the Fennoscandian Shield was formed and subject to major metamorphic and deformational reworking 2.6–2.9 Ga ago. The Archean metamorphic event was followed by the Lapland-Kola collisional orogenesis, which included intracontinental rifting of an Archean crust (2.5–2.1 Ga), Red Sea-type oceanic separation (~2.1–2.0 Ga), subduction and crustal growth (~2.0–1.9 Ga), intercontinental collision (1.94–1.86 Ga) and orogenic collapse and exhumation (1.90–1.86 Ga) [5,16,21].

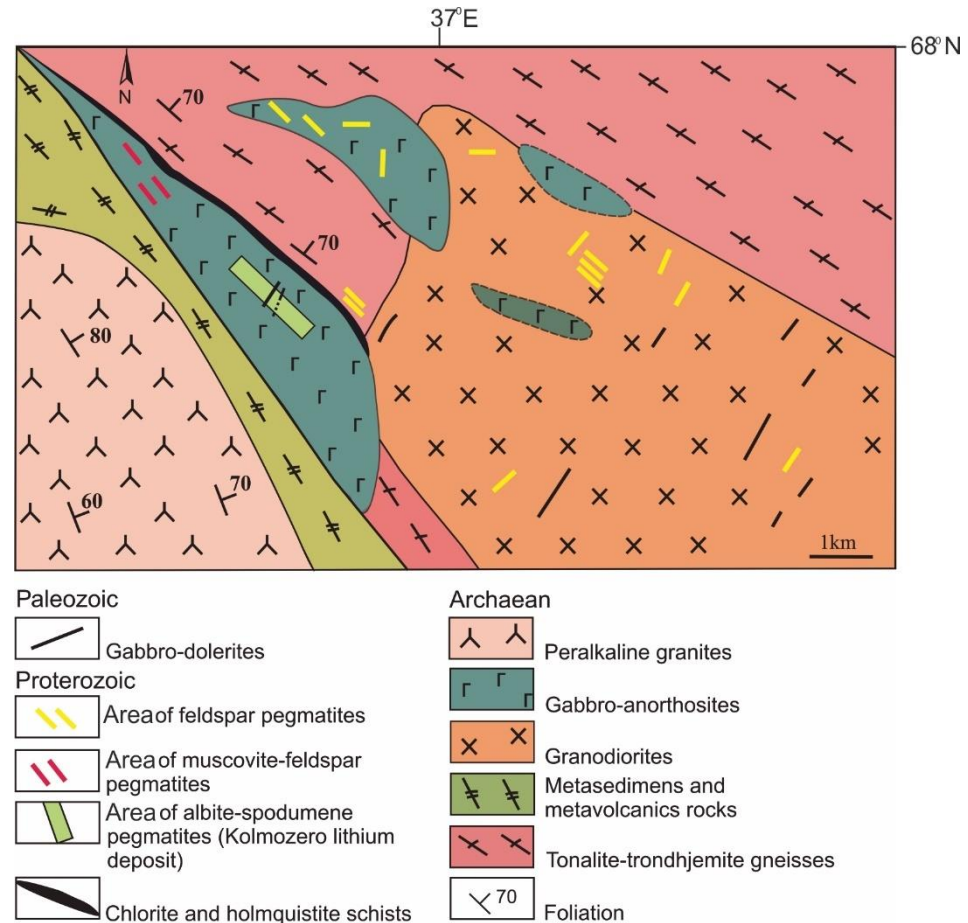


Figure 2. Schematic geological map of the Kolmozero pegmatite field. Modified after Morozova [15].

The Kolmozero pegmatite field occurs in the tonalite-trondhjemite gneisses of the Murmansk province, which were intruded by the Kolmozero massif at about 2.73 Ga (metagabbrodiorites, metamonzodiorites, and metagranodiorites) [22] and by the metagabbro-anorthosite massifs of Severny, Bezmyanny and Patchemvarek at about 2.66 Ga [23]. The albite-spodumene pegmatites were emplaced into the Patchemvarek massif at 2.315 ± 0.01 Ga [24]. These pegmatites are cross-cut by Palaeozoic (?) gabbro-dolerite dikes. The muscovite-feldspar pegmatites of unknown geochronological age intruded on the Bezmyanny massif northwest of the Kolmozero deposit. The feldspar pegmatites are located north of the Kolmozero deposit in the Severny massif and tonalite-trondhjemite gneisses (Figure 2). Cross-cutting relationships between these different pegmatites were not observed and, thus, the sequence of pegmatite emplacement remains unclear.

2.2. Kolmozero Pegmatite Field

The Kolmozero Li deposit forms part of the Kolmozero pegmatite field and consists of 12 albite-spodumene pegmatite dykes and numerous small occurrences. The largest dykes have lengths of over 1400 m and thicknesses up to 65 m and extend to depths of about 500 m. The pegmatite dykes do not display a mineralogical zoning at this scale of observation and comprise quartz (30–35 vol.%), albite (30–35 vol.%), K-feldspar (10–25 vol.%), spodumene

(~20 vol.%), and muscovite (5–7 vol.%). Spodumene is the main host for lithium with 97% of the bulk rock Li_2O in the Kolmozero pegmatites (Figure 3), 0.3% is carried by lithiophilite, 0.45% by muscovite, 1.93% by albite and 0.3% by K-feldspar. Beryl and columbite-group minerals are accessory and may have commercial by-product potential as a source for Be, Ta, and Nb. Other accessory minerals include spessartine, apatite, rare lithiophilite, triphylite, and tourmaline. Internal structures of the dykes are very simple where 85 to 90 vol.% of the dykes are composed of medium to coarse-grained quartz, spodumene, albite, muscovite, and megacrystic (blocky) K-feldspar. Individual spodumene crystals can reach up to 1.5 m in length. Megacrystic K-feldspar is up to 40–60 cm across, cleavelandite up to 10 cm in length and muscovite up to 15 cm across. Li_2O content in albite-spodumene pegmatites varies from 0.5 to 2.66 wt.% [14,15,25]. Aplitic and coarse-grained quartz-plagioclase domains are developed at the margins of the pegmatite dykes in contact with the country rocks. Geochemically, the Kolmozero albite-spodumene pegmatites correspond to the rare-metal pegmatites of the LCT (lithium-cesium-tantalum) family according to [26].

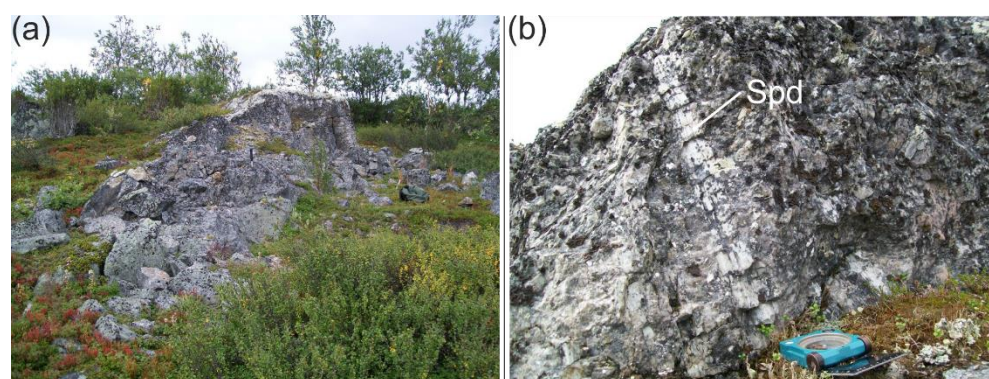


Figure 3. (a) Exposure of an albite-spodumene pegmatite dyke of the Kolmozero deposit. (b) Spodumene (Spd) crystals in an albite-spodumene pegmatite of the Kolmozero deposit.

Dykes of feldspar and muscovite-feldspar pegmatite also occur in the Kolmozero pegmatite field (Figure 2). Feldspar pegmatites have a simple mineral composition and consist of quartz (30–40 vol.%), K-feldspar (30–60 vol.%), and plagioclase (10–30 vol.%). Accessory minerals: muscovite, spessartine, ilmenite, magnetite, rare beryl, columbite-group minerals, biotite, tourmaline, and molybdenite. Muscovite-feldspar pegmatites consist of quartz (25–30 vol.%), K-feldspar (35–50 vol.%), plagioclase (15–30 vol.%), and muscovite (5–12 vol.%). Accessory minerals include beryl, columbite-group minerals, spessartine, apatite and extremely rare spodumene. Internal structures within the muscovite-feldspar and feldspar pegmatite are simple, showing no pronounced concentric mineralogical or textural variability. The margins of the dykes are, however, commonly fine-grained. The main part of the muscovite-feldspar pegmatites (90–95 vol.%) is composed of medium- to coarse-grained and megacrystic quartz, muscovite and feldspar. Feldspar pegmatites are mainly composed of medium-grained to megacrystic quartz and feldspar [14].

3. Analytical Methods and Sampling

3.1. Electron Microprobe Analyses

Electron microprobe analyses was performed using a Cameca MS-46 (EMPA) (Cameca, Gennevilliers, France) instrument at the Geological Institute of the Kola Science Center of the Russian Academy of Sciences (Apatity, Russia) (GI KSC RAS). The instrument was operated in a wavelength-dispersive mode in the following conditions: acceleration voltage 22 kV, beam current 20–40 nA, and 50 s counting time. The following standards and analytical lines were used for the analysis of the K-feldspar: wollastonite ($\text{SiK}\alpha$), wadeite ($\text{KK}\alpha$), and $\text{Y}_3\text{Al}_5\text{O}_{12}$ ($\text{AlK}\alpha$). Detection limits for Si, Al, and K were 0.02%.

The study of the internal structure of the K-feldspar and qualitative composition of the mineral inclusions was carried out using a LEO-1450 SEM (scanning electron microscope)

(Carl Zeiss AG, Oberkochen, Germany) equipped with an XFlash-5010 Bruker Nano GmbH EDS (energy-dispersive X-ray spectroscopy) detector at the Geological Institute KSC RAS. The system was operated at 20 kV acceleration voltage, 0.5 nA beam current, with 200 s accumulation time.

Petrographic studies were carried out with an Axioplan-2 Imaging microscope equipped with a digital camera and the image processing system (Carl Zeiss MicroImaging GmbH, Goettingen, Germany) at the Geological Institute KSC RAS.

3.2. LA-ICP-MS Analyses

Trace element mineral chemistry of the K-feldspar were determined by laser ablation inductively coupled plasma mass spectrometry (LA-ICP-MS) using a NexION 300S PerkinElmer instrument with an attached NWR 213 laser at the Geoanalytik Core Facilities Centre of the Institute of Geology and Geochemistry of the Urals Branch of the Russian Academy Sciences (Yekaterinburg, Russia). The analyses were carried out at an ISO class 7 clean room. The laser ablation was performed at a pulse repetition rate of 12 Hz and laser energy density 10.5–11.5 J/cm² in a spot (crater diameter) 50 µm in size. The results were processed using the GLITTER V4.4 software (GEMOC, Macquarie University, Australia) and applying the stoichiometric SiO₂ content as an internal standard. NIST SRM 610 glass was measured as the primary external standard after each 10–12 analyses of K-feldspar. NIST SRM 612 glass was used as a secondary standard. Concentrations were determined for the following elements: Li, Be, B, Na, Mg, Ca, Sc, Ti, V, Cr, Fe, Mn, Co, Ni, Cu, Zn, Ga, Ge, As, Se, Rb, Sr, Y, Zr, Nb, Mo, Ag, Cd, In, Sn, Sb, Te, Cs, Ba, REE, Hf, Ta, W, Tl, Pb, Bi, Th, and U. LA-ICP-MS analyses of K-feldspar were obtained on the polished thin sections of 110–130 µm thickness.

3.3. Powder X-ray Diffraction

Powder X-ray diffraction measurements of the K-feldspar grains were performed with a DRON-2 diffractometer (Russia) at the Geological Institute of the Kola Science Center of the Russian Academy of Sciences (Apatity, Russia). The operating parameters were as follows: CuK α radiation, 20 mA, 30 kV. The Powder X-ray diffraction patterns were collected in the range of angles 2 θ from 10 to 67° with a rate of 1° per minute and in the range of angles 2 θ 20–32° and 40–52° with a rate of 0.5° per minute. Powder X-ray diffraction data for the K-feldspar were identified using the RRUFF Project database [27]).

3.4. K-Feldspar Samples

The samples were selected to represent variations in the chemical composition and structural state of megacrystic blocky K-feldspars from albite-spodumene pegmatites. Based on the crystal morphology, texture, and mineral associations, two different megacrystic K-feldspar types (microcline-I (Mc-I) and microcline-II (Mc-II)) were identified in the Kolmozero deposit [14]; this article). Microcline-I occurs in the wall zone of the dikes in association with coarse-grained albite and quartz, and is represented by opaque, greyish-pink crystals up to 10 cm across. In microcline-I, the microscopic investigation revealed micro-perthite texture and tartan twinning (chess-board patterns) (Figure 4a). Microcline-II is most common in albite-spodumene pegmatites. In intermediate parts of the dykes, aggregate of megacrystic greyish-pink microcline-II up to 40–60 cm across composes separated areas, with the size of 5 m \times 2 m, in association with a coarse- and giant-grained quartz-spodumene-albite aggregate. Petrographic investigation of microcline-II revealed the cryptoperthitic texture (Figure 4b,c). Mineral inclusions in microcline-I and microcline-II include albite, quartz, and muscovite. Rare quartz-microcline-albite and quartz-albite veinlets intersect microcline crystals. Rims of microcline-I and microcline-II are partly replaced by saccharoidal albite and fine-grained microcline.

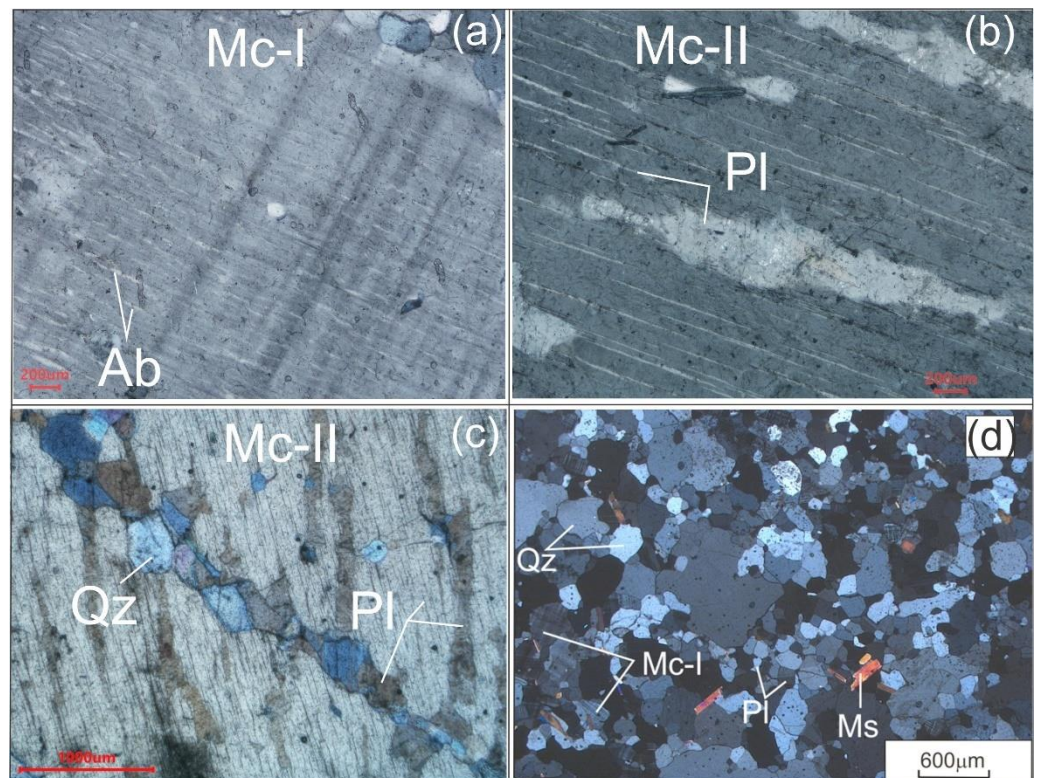


Figure 4. (a) Photomicrographs (plane polarized light) of Mc-I sections from albite-spodumene pegmatites. In Mc-I, microscopic investigation revealed micro-perthite texture (b,c). Photomicrographs (plane polarized light) of Mc-II sections from albite-spodumene pegmatites. Microscopic investigation reveals micro-perthite texture in Mc-II. Plagioclase in (b) forms vein perthite and film perthite. The quartz-plagioclase veinlet in (c) intersects the perthite texture in Mc-II. (d) Photomicrographs (plane polarized light) of Mc-I sections from feldspar pegmatites. Ab, albite; Qz, quartz; Pl, plagioclase; Mc, microcline; Ms, muscovite.

For comparison, samples of perthitic megacrystic K-feldspar (microcline-II (Mc-II)) from the central part of the feldspar pegmatite dykes and samples of fine-grained K-feldspar (microcline-I (Mc-I)) from the margin of the dykes (Figure 4d) were investigated. Mineral inclusions in microcline-II include albite, quartz, and muscovite. The quartz-microcline-plagioclase and quartz-plagioclase veinlets intersect megacrystic blocky microcline-II. Microcline-II is replaced by saccharoidal albite and fine-grained microcline.

4. Results

4.1. Structural States

Microcline $KAlSi_3O_8$ relates to framework aluminosilicates. The crystal structure of feldspar commonly occurs as an aluminosilicate framework, in which interstices are occupied by alkali and alkali-earth atoms. The general feldspar formula is MT_4O_8 , where M comprises large cations (e.g., Na, K, Ca) filling interstices in the framework structure, and T (atoms in tetrahedral coordination with oxygen—Al, Si, B and Fe^{3+}) composing the frame in the tetrahedral site [28–30].

Structural features of three K-feldspar samples were examined by powder X-ray diffraction techniques. X-ray phase analysis showed that K-feldspars from albite-spodumene and feldspar pegmatites are mainly composed of microcline and have an additional sodium phase (Figure 5).

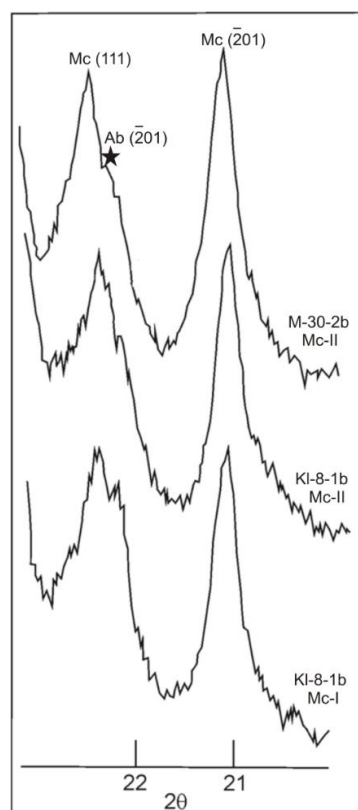


Figure 5. The (201) diffraction of K-feldspars in pegmatites from the Kolmozero field. M-30-2b (Mc-I) represents a K-feldspar from feldspar pegmatites and KI-8-1b (Mc-I) and KI-125-1 (Mc-II) originate from albite-spodumene pegmatites. X-ray phase analysis showed that K-feldspars from albite-spodumene and feldspar pegmatites mainly contain a microcline (Mc) and an additional Na phase (Ab).

4.2. Geochemistry of K-Feldspar from Albite-Spodumene Pegmatites

Representative compositions of K-feldspar from albite-spodumene pegmatites and feldspar pegmatites determined by electron microprobe analysis are provided in Tables 1 and 3, and determined by the LA-ICP-MS method are provided in Tables 2 and 4. Chemical formulas of the K-feldspar from EMPA were calculated based on the oxygen method ($O = 8$) using the theoretical formula $M(T_4O_8)$ [30].

In addition to Al, K, and Na, K-feldspar from albite-spodumene pegmatites contains minor and trace elements, including Rb, Cs, Li, and Tl. Microcline-II differs from microcline-I by having a relatively higher concentration of Rb (average 6720 and 4486 ppm, respectively), Cs (146 and 92 ppm, respectively), Li (86.3 and 67.9 ppm, respectively), and Tl (34 and 28 ppm, respectively) (Figure 6). Manganese ranges from 0.95 to 14.3 ppm in microcline-I. In microcline-II, Mn varies from 3.0 to 16.5 ppm. The average Pb, Sr, and Ba contents decrease from microcline-I (26.3, 23.6 and 29.5 ppm, respectively) to microcline-II (13.6, 8.4 and 13.4 ppm, respectively) (Figure 6).

In albite-spodumene pegmatites, Ta is present in very low concentrations ranging from 0.07 (microcline-I) to 0.41 (microcline-II) ppm. The average Be content in microcline-I and microcline-II ranges from 5 to 3 ppm, respectively, while Nb varies from 0.04 to 3.3 ppm, respectively. Microcline-II and microcline-I have identical contents of Ga (19.1 and 19.9 ppm, respectively) and Ge (4.2 and 4.9 ppm, respectively). The contents of other trace elements are variable

Table 1. Representative chemical composition (wt.%) and mineral formulae (apfu) of K-feldspar from the albite-spodumene pegmatites determined by electron microprobe analysis.

Type Sample	Microcline-I					Microcline-II								
	KI-8-2a	KI-8-2b	KI-8-2c	KI-8-1b	KI-8-1c	KI-121/7	KI-121/8	KI-121/6	KI-125/5	KI-125/1	KI-125/2	KI-125/3	KI-125/4	
SiO ₂ ‡	64.95	64.88	64.75	64.94	64.88	64.88	64.67	64.85	64.64	64.67	64.66	64.69	64.79	
Al ₂ O ₃ ‡	18.33	18.31	18.29	18.36	18.247	18.29	18.27	18.29	18.29	18.25	18.29	18.26	18.29	
CaO †	b.d.	b.d.	b.d.	b.d.	b.d.	b.d.	b.d.	b.d.	b.d.	b.d.	b.d.	b.d.	b.d.	
Na ₂ O †	0.48	0.47	0.53	0.42	0.48	0.23	0.32	0.32	0.39	0.27	0.36	0.33	0.38	
K ₂ O ‡	15.92	15.90	16.01	16.01	15.99	15.66	16.00	16.04	15.89	16.09	15.90	16.03	15.87	
Rb ₂ O †	0.49	0.52	0.48	0.48	0.47	0.72	0.75	0.67	0.78	0.73	0.78	0.66	0.81	
Cs ₂ O †	0.011	0.011	0.009	0.009	0.009	0.015	0.016	0.015	0.015	0.015	0.019	0.015	0.015	
Li ₂ O †	0.013	0.016	0.016	0.018	0.011	0.020	0.026	0.018	0.022	0.013	0.019	0.012	0.019	
Total	100.2	100.1	100.1	100.2	100.1	100.0	100.0	100.2	100.0	100.0	100.0	100.0	100.2	
Formulae of the basis of 8 O														
T	Si ⁴⁺	3.001	3.001	2.999	3.000	3.003	3.001	3.000	3.002	2.999	3.001	2.999	3.001	3.001
	Al ³⁺	0.999	0.998	0.998	0.999	0.995	0.997	0.999	0.998	1.000	0.998	1.000	0.998	0.998
	ΣT	4.000	3.999	3.997	3.999	3.998	3.998	3.999	3.999	3.999	3.999	3.999	3.999	3.999
	Ca ²⁺	b.d.	b.d.	b.d.	b.d.	b.d.	b.d.	b.d.	b.d.	b.d.	b.d.	b.d.	b.d.	b.d.
M	Na ⁺	0.043	0.0426	0.047	0.037	0.043	0.021	0.029	0.029	0.035	0.024	0.032	0.029	0.034
	K ⁺	0.939	0.9399	0.946	0.944	0.945	0.924	0.947	0.947	0.941	0.953	0.941	0.949	0.938
	Rb ⁺	0.0155	0.015	0.014	0.014	0.014	0.021	0.022	0.019	0.023	0.022	0.023	0.019	0.024
	Cs ⁺	b.d.	b.d.	b.d.	b.d.	b.d.	b.d.	b.d.	b.d.	b.d.	b.d.	b.d.	b.d.	b.d.
	Li ⁺	0.002	0.003	0.003	0.003	0.002	0.038	0.005	0.003	0.004	0.003	0.004	0.002	0.004
	ΣM	1.000	1.001	1.010	0.998	1.004	1.004	1.003	0.998	1.003	1.002	1.000	0.999	1.000
Basic minerals (mol.%)														
Ab	4.36	4.34	4.76	3.80	4.32	2.20	2.92	2.95	3.58	2.44	3.32	3.02	3.48	
An	b.d.	b.d.	b.d.	b.d.	b.d.	b.d.	b.d.	b.d.	b.d.	b.d.	b.d.	b.d.	b.d.	
Or	95.64	95.66	95.24	96.20	95.68	97.80	97.08	97.05	96.42	97.56	96.68	96.98	96.52	

‡ Determined by EMPA; † Determined by LA-ICP-MS; b.d., below detection limit.

Table 2. Minor and trace elements in the K-feldspar from highly fractionated albite-spodumene pegmatites (ppm) determined by LA-ICP-MS.

Element	Microcline-1						Microcline-II								
	K1-8-2a	K1-8-2b	K1-8-2c	K1-8-1b	K1-8-1c	Average	K1-121/7	K1-121/8	K1-121/6	K1-125/5	K1-125/1	K1-125/2	K1-125/3	K1-125/4	Average
Li	59.75	73.34	73.27	83.61	49.45	67.88	94.45	120.4	84.04	99.74	61.51	87.2	56.49	86.23	86.26
Be	b.d.	3.84	b.d.	b.d.	5.86	4.85	1.34	b.d.	4.28	4.96	0.99	b.d.	b.d.	3.54	3.02
Ta	0.09	0.09	b.d.	0.02	b.d.	0.07	0.022	b.d.	0.07	b.d.	0.06	b.d.	b.d.	1.50	0.41
Nb	0.06	0.04	b.d.	b.d.	b.d.	0.05	b.d.	b.d.	b.d.	b.d.	b.d.	b.d.	b.d.	3.32	3.32
Rb	4527	4733	4414	4418	4337	4486	6595	6825	6089	6940	6684	7172	6051	7403	6720
Cs	100.8	98.6	92.9	83.1	82.1	91.5	137.9	147.1	136.5	140.6	141.6	174.2	145.5	143	145.8
Sr	23.6	31.1	20.5	20.2	22.5	23.6	10.8	6.67	10.1	10.8	7.85	7.56	7.41	12.1	8.41
Ba	48	26.2	25.6	26.2	21.5	29.5	16	11.4	12.8	11.7	12.4	19.9	13.3	9.61	13.4
Tl	29.9	30.9	29.3	25.9	24.3	28.1	34.5	33.6	32.5	35.2	30.3	36.8	32.2	37.9	34.1
Pb	16.8	22.3	35.1	28.3	29.1	26.3	17.6	11.8	15	19.3	6.35	18.9	11.7	7.81	13.6
Ga	16.9	20.6	15.7	14.7	15.9	16.8	19.1	19.1	19.9	21.3	17.2	18.4	17.6	26.7	19.9
Ge	4.32	4.22	2.07	4.06	6.84	4.30	4.24	5.17	6.77	5.87	3.77	3.10	4.66	5.84	4.93
Mn	0.95	4.17	14.29	7.85	5.30	6.51	3.01	15.48	2.19	7.20	16.54	1.59	2.69	11.84	7.57
Sc	0.40	1.00	0.76	b.d.	0.95	0.78	0.9	0.95	b.d.	1.06	1.34	0.66	0.67	0.74	0.90
B	2.13	3.20	1.69	b.d.	b.d.	2.34	3.09	6.87	2.15	b.d.	b.d.	4.32	2.04	b.d.	3.69
Mg	b.d.	b.d.	b.d.	b.d.	b.d.	b.d.	0.51	b.d.	b.d.	33.21	b.d.	b.d.	93.15	51.65	44.63
Ti	b.d.	3.91	b.d.	3.90	1.34	3.05	b.d.	2.90	b.d.	b.d.	b.d.	3.62	b.d.	9.22	5.25
V	b.d.	b.d.	b.d.	b.d.	b.d.	b.d.	0.14	b.d.	0.05	b.d.	b.d.	b.d.	b.d.	b.d.	0.09
Cr	b.d.	6.36	7.81	4.21	4.66	5.76	b.d.	7.56	4.81	b.d.	6.88	b.d.	9.06	b.d.	7.08
Fe	b.d.	b.d.	61.69	26.20	b.d.	43.95	b.d.	16.79	b.d.	44.68	37.00	b.d.	16.54	21.22	27.26
Co	b.d.	b.d.	b.d.	b.d.	b.d.	b.d.	0.44	b.d.	0.44						
Ni	b.d.	0.32	b.d.	b.d.	b.d.	0.32	b.d.	0.88	0.31	b.d.	b.d.	0.38	b.d.	b.d.	0.52
Cu	5.38	3.00	3.98	8.95	1.57	4.58	1.65	1.42	1.23	b.d.	b.d.	b.d.	1.21	0.80	1.26
Zn	b.d.	b.d.	b.d.	b.d.	1.28	1.28	b.d.	b.d.	b.d.	b.d.	b.d.	b.d.	b.d.	2.32	2.32
As	b.d.	b.d.	1.37	b.d.	b.d.	1.37	b.d.	b.d.	b.d.	b.d.	b.d.	b.d.	b.d.	b.d.	b.d.
Se	b.d.	b.d.	b.d.	b.d.	b.d.	b.d.	b.d.	b.d.	b.d.	24.39	22.16	b.d.	b.d.	b.d.	23.28
Y	b.d.	b.d.	b.d.	0.10	b.d.	0.01	0.04	b.d.	b.d.	b.d.	0.11	b.d.	0.16	b.d.	0.10
Zr	0.12	b.d.	b.d.	b.d.	b.d.	0.12	b.d.	b.d.	b.d.	b.d.	0.23	b.d.	0.61	0.41	0.42
Mo	b.d.	0.23	b.d.	b.d.	b.d.	0.046	b.d.	b.d.	0.23	b.d.	b.d.	b.d.	b.d.	b.d.	0.029
Ag	b.d.	0.20	b.d.	b.d.	b.d.	0.20	1.92	0.15	b.d.	b.d.	b.d.	b.d.	b.d.	b.d.	1.04
Cd	b.d.	0.10	b.d.	b.d.	b.d.	0.10	b.d.	b.d.	0.11	b.d.	b.d.	b.d.	b.d.	1.13	0.62
In	b.d.	b.d.	0.02	b.d.	0.02	0.02	b.d.	b.d.	b.d.	b.d.	0.02	b.d.	b.d.	0.06	0.04
Sn	0.28	b.d.	b.d.	b.d.	b.d.	0.28	0.57	b.d.	0.70	0.62	b.d.	b.d.	b.d.	10.56	3.11
Sb	b.d.	b.d.	b.d.	b.d.	b.d.	b.d.	0.17	b.d.	b.d.	0.10	0.36	b.d.	0.31	b.d.	0.24

Table 2. Cont.

Element	Microcline-1						Microcline-II								
	KI-8-2a	KI-8-2b	KI-8-2c	KI-8-1b	KI-8-1c	Average	KI-121/7	KI-121/8	KI-121/6	KI-125/5	KI-125/1	KI-125/2	KI-125/3	KI-125/4	Average
La	b.d.	b.d.	0.05	b.d.	b.d.	0.01	b.d.	b.d.	b.d.	b.d.	b.d.	b.d.	0.07	0.05	0.015
Ce	b.d.	b.d.	b.d.	b.d.	b.d.	b.d.	b.d.	b.d.	b.d.	b.d.	b.d.	b.d.	0.33	0.15	0.24
Pr	b.d.	b.d.	b.d.	b.d.	b.d.	b.d.	b.d.	b.d.	b.d.	b.d.	b.d.	b.d.	0.10	b.d.	0.10
Nd	b.d.	b.d.	b.d.	b.d.	b.d.	b.d.	0.1	0.16	b.d.	0.24	b.d.	b.d.	0.12	b.d.	0.16
Sm	b.d.	b.d.	b.d.	b.d.	b.d.	b.d.	b.d.	b.d.	b.d.	b.d.	b.d.	b.d.	b.d.	b.d.	b.d.
Eu	b.d.	b.d.	b.d.	b.d.	b.d.	b.d.	b.d.	b.d.	b.d.	b.d.	b.d.	b.d.	b.d.	b.d.	b.d.
Gd	b.d.	b.d.	b.d.	b.d.	b.d.	b.d.	b.d.	0.13	b.d.	b.d.	b.d.	b.d.	b.d.	b.d.	0.13
Tb	b.d.	b.d.	b.d.	b.d.	b.d.	b.d.	b.d.	b.d.	b.d.	b.d.	b.d.	b.d.	b.d.	b.d.	b.d.
Dy	b.d.	b.d.	b.d.	b.d.	b.d.	b.d.	b.d.	b.d.	b.d.	b.d.	b.d.	b.d.	b.d.	b.d.	b.d.
Ho	b.d.	b.d.	b.d.	b.d.	b.d.	b.d.	b.d.	b.d.	b.d.	b.d.	b.d.	b.d.	b.d.	b.d.	b.d.
Er	b.d.	b.d.	b.d.	b.d.	b.d.	b.d.	b.d.	b.d.	b.d.	0.11	b.d.	b.d.	b.d.	b.d.	0.11
Tm	b.d.	b.d.	b.d.	b.d.	b.d.	b.d.	b.d.	b.d.	b.d.	b.d.	b.d.	b.d.	b.d.	b.d.	b.d.
Yb	b.d.	b.d.	b.d.	b.d.	b.d.	b.d.	b.d.	b.d.	b.d.	0.10	b.d.	b.d.	b.d.	b.d.	0.10
Lu	b.d.	b.d.	b.d.	b.d.	b.d.	b.d.	b.d.	0.03	b.d.	b.d.	b.d.	b.d.	b.d.	b.d.	0.03
Hf	b.d.	b.d.	b.d.	b.d.	0.07	0.07	b.d.	0.09	b.d.	b.d.	b.d.	b.d.	0.13	b.d.	0.11
W	b.d.	b.d.	b.d.	b.d.	b.d.	b.d.	b.d.	b.d.	b.d.	b.d.	b.d.	b.d.	b.d.	0.18	0.18
Bi	b.d.	0.09	0.18	b.d.	b.d.	0.14	b.d.	b.d.	b.d.	b.d.	b.d.	b.d.	b.d.	0.03	0.03
Th	b.d.	b.d.	0.06	b.d.	b.d.	0.06	b.d.	0.04	0.02	0.03	6.07	0.03	0.03	0.16	0.91
U	b.d.	0.02	b.d.	b.d.	b.d.	0.02	b.d.	b.d.	b.d.	b.d.	b.d.	b.d.	0.04	0.44	0.24

b.d., below detection limit; data obtained by the LA-ICP-MS method.

Table 3. Representative chemical composition (wt.%) and mineral formulae (apfu) of K-feldspar from the feldspar pegmatites determined by electron microprobe analysis.

Type Sample No.	Microcline-I					Microcline-II				
	M-30/1	M-30/4	KI-20/1	KI-20/2	KI-20/3	KI-5/1	KI-5/2	KI-5/3	M-30/2	M-30/3
SiO ₂ †	64.89	64.89	64.97	64.98	64.93	64.84	64.88	64.89	64.89	64.89
Al ₂ O ₃ †	18.39	18.26	18.28	18.29	18.27	18.29	18.29	18.29	18.28	18.29
CaO †	b.d.	b.d.	b.d.	0.09	b.d.	0.11	0.08	0.07	0.07	0.05
Na ₂ O †	0.74	0.59	0.77	0.79	0.68	0.42	0.41	0.57	0.54	0.51
K ₂ O †	15.58	15.88	15.56	15.58	15.73	16.18	16.16	16.01	16.07	16.11
Rb ₂ O †	0.03	0.03	0.03	0.03	0.03	0.11	0.15	0.14	0.14	0.13
SrO †	0.04	0.04	0.04	0.04	0.04	0.01	0.01	0.01	0.01	0.01

Table 3. Cont.

Type	Sample No.	Microcline-I				Microcline-II					
		M-30/1	M-30/4	KI-20/1	KI-20/2	KI-20/3	KI-5/1	KI-5/2	KI-5/3	M-30/2	M-30/3
BaO [†]		0.53	0.49	0.49	0.47	0.47	0.03	0.32	0.03	0.02	0.03
Total		100.2	100.2	100.2	100.3	100.2	99.9	99.9	100.0	100.0	100.0
Formulae on the basis of 8 O											
T	Si ⁴⁺	2.997	3.001	3.002	2.999	3.001	2.999	3.001	3.000	3.001	3.006
	Al ³⁺	1.002	0.995	0.995	0.995	0.995	0.998	0.997	0.997	0.996	0.997
ΣT		3.999	3.996	3.997	3.994	3.997	3.998	3.998	3.997	3.997	3.998
M	Ca ²⁺	b.d.	b.d.	b.d.	0.005	b.d.	0.005	0.004	0.003	0.003	0.003
	Na ⁺	0.066	0.053	0.069	0.072	0.061	0.038	0.036	0.052	0.048	0.046
	K ⁺	0.918	0.937	0.917	0.918	0.928	0.955	0.954	0.944	0.948	0.950
	Rb ⁺	0.001	0.001	0.001	0.001	0.001	0.003	0.004	0.004	0.004	0.004
	Sr ²⁺	0.001	0.001	0.001	0.001	0.001	b.d.	b.d.	b.d.	b.d.	b.d.
ΣM	Ba ²⁺	0.009	0.009	0.0089	0.008	0.007	0.001	0.001	0.001	b.d.	0.001
		0.996	1.000	0.997	1.004	0.999	1.002	1.002	1.004	1.004	1.003
Basic minerals (mol.%)											
Ab		6.74	5.34	6.99	7.19	6.18	3.80	3.66	5.15	4.83	4.56
An		b.d.	b.d.	b.d.	0.45	b.d.	0.54	0.39	0.33	0.32	0.26
Or		93.26	94.66	93.01	92.35	93.82	95.66	95.95	94.51	94.85	95.18

[‡] Determined by EMPA; [†] Determined by LA-ICP-MS; b.d., below detection limit.

Table 4. Minor and trace elements in the K-feldspar from the feldspar pegmatites (ppm) determined by LA-ICP-MS.

Element	M-30/1	M-30/4	Microcline-I				Average	Microcline-II				Average
			KI-20/1	KI-20/2	KI-20/3	KI-5/1		KI-5/2	KI-5/3	M-30/2	M-30/3	
Li	7.22	14.47	17.9	15.19	13.9	13.74	18.56	15.79	14.37	17.56	20.14	17.28
Be	b.d.	b.d.	b.d.	b.d.	b.d.	b.d.	b.d.	1.75	b.d.	b.d.	b.d.	1.75
Ta	0.32	0.75	0.59	0.36	0.50	0.50	2.65	b.d.	0.184	0.021	0.312	0.79
Nb	0.19	b.d.	b.d.	b.d.	0.092	0.09	15.98	b.d.	b.d.	0.062	b.d.	8.02
Rb	302.1	298.3	285.4	280.3	314.5	296.1	1004	1368	1261	1248	1143	1205
Cs	8.13	6.75	7.01	6.66	7.47	7.20	18.24	29.5	24.15	27.51	25.26	24.93
Sr	367.2	325.1	332.8	340.2	336.5	340.4	30.5	30.4	88.8	53.7	70.2	54.7
Ba	4736	4407	4408	4169	4241	4392	235.3	293.7	305.3	209.7	255.2	259.8

Table 4. Cont.

Element	Microcline-I						Microcline-II					
	M-30/1	M-30/4	KI-20/1	KI-20/2	KI-20/3	Average	KI-5/1	KI-5/2	KI-5/3	M-30/2	M-30/3	Average
Tl	1.59	1.83	1.6	1.7	1.43	1.63	5.83	7.61	5.78	6.1	5.52	6.17
Pb	59	54.9	50.9	53.5	58.2	55.3	24	39.5	32.7	27.1	29.2	30.5
Ga	12.9	13.1	13.3	12	14.4	13.1	24.7	21.6	21.6	25.5	24.5	23.6
Ge	2.93	b.d.	b.d.	b.d.	1.35	2.14	5.56	b.d.	3.7	4.21	2.23	3.93
Mn	2.21	1.14	1.54	1.41	1.46	1.55	3.51	b.d.	4.89	0.69	1.81	2.73
Sc	b.d.	b.d.	0.56	0.58	0.7	0.61	0.75	b.d.	b.d.	b.d.	0.27	0.51
B	3.48	4.54	5.76	4.79	2.92	4.30	b.d.	b.d.	6.65	b.d.	4.74	5.70
Mg	22.1	b.d.	45.6	b.d.	b.d.	38.9	127.4	b.d.	b.d.	b.d.	b.d.	127.4
Ca	b.d.	b.d.	197.4	650.9	b.d.	424.2	778.5	557.9	483	110.5	371.4	460.3
Ti	4.14	7.88	7.25	5.83	9.86	6.99	8.67	7.87	4.29	3.12	2.41	5.27
V	b.d.	b.d.	b.d.	b.d.	b.d.	b.d.	0.181	b.d.	b.d.	0.2	0.24	0.21
Cr	12.91	b.d.	11.62	5.91	5.25	8.92	12.02	8.2	4.63	5.41	4.41	6.93
Fe	86.9	61.8	55.8	45.6	80.7	66.2	96.3	64.9	107.7	29.9	b.d.	74.7
Ni	b.d.	b.d.	b.d.	0.27	b.d.	0.27	b.d.	b.d.	b.d.	0.75	0.68	0.72
Cu	b.d.	5.91	b.d.	1.79	1.3	3.00	84.7	1.34	40	9	29.1	32.8
Zn	b.d.	b.d.	b.d.	b.d.	b.d.	b.d.	14.1	b.d.	b.d.	b.d.	b.d.	14.1
As	2.82	b.d.	1.58	b.d.	b.d.	2.20	b.d.	b.d.	1.28	b.d.	1.46	1.37
Y	b.d.	0.23	0.25	b.d.	0.103	0.19	0.55	0.52	0.11	0.13	0.25	0.31
Zr	b.d.	b.d.	b.d.	b.d.	b.d.	b.d.	11.66	b.d.	b.d.	0.38	b.d.	6.02
Mo	0.47	0.25	b.d.	b.d.	b.d.	0.36	b.d.	0.49	b.d.	0.2	b.d.	0.35
Ag	b.d.	b.d.	b.d.	b.d.	b.d.	b.d.	0.45	0.24	b.d.	b.d.	0.18	0.29
Cd	b.d.	b.d.	b.d.	b.d.	0.11	0.11	0.22	b.d.	b.d.	b.d.	b.d.	0.22
In	b.d.	0.018	0.016	b.d.	b.d.	0.02	b.d.	b.d.	b.d.	b.d.	b.d.	b.d.
Sn	0.39	b.d.	b.d.	b.d.	0.47	0.43	0.57	0.51	b.d.	0.66	b.d.	0.58
Sb	b.d.	b.d.	0	0.071	0.09	0.08	0.24	b.d.	b.d.	b.d.	b.d.	0.24
La	b.d.	b.d.	0.058	b.d.	b.d.	0.06	0.53	0.176	0.311	0.51	0.45	0.40
Ce	0.056	b.d.	b.d.	b.d.	b.d.	0.06	1.07	0.14	0.51	0.7	1.19	0.72
Pr	b.d.	0.018	b.d.	b.d.	b.d.	0.02	0.142	b.d.	0.033	0.059	0.137	0.09
Nd	b.d.	b.d.	b.d.	0.085	b.d.	0.09	0.55	0.23	0	0.095	0.17	0.209
Sm	b.d.	b.d.	b.d.	b.d.	b.d.	b.d.	b.d.	b.d.	b.d.	b.d.	b.d.	b.d.
Eu	0.098	0.208	0.25	0.227	0.255	0.202	b.d.	b.d.	b.d.	0.112	0.097	0.10
included intraconti- nental	b.d.	b.d.	b.d.	0.068	0.07	b.d.	0.33	0.37	0.084	b.d.	b.d.	0.26
Gd												
Tb	b.d.	b.d.	b.d.	b.d.	b.d.	b.d.	0.039	b.d.	b.d.	b.d.	0.02	0.03

Table 4. Cont.

Element	Microcline-I						Microcline-II					
	M-30/1	M-30/4	KI-20/1	KI-20/2	KI-20/3	Average	KI-5/1	KI-5/2	KI-5/3	M-30/2	M-30/3	Average
Dy	b.d.	b.d.	b.d.	b.d.	b.d.	b.d.	0.053	0.18	b.d.	b.d.	b.d.	0.12
Ho	b.d.	b.d.	b.d.	b.d.	b.d.	b.d.	b.d.	0.047	b.d.	b.d.	b.d.	0.05
Er	b.d.	b.d.	b.d.	b.d.	b.d.	b.d.	b.d.	b.d.	b.d.	b.d.	0.093	0.09
Tm	b.d.	b.d.	b.d.	b.d.	b.d.	b.d.	b.d.	b.d.	b.d.	b.d.	b.d.	b.d.
Yb	b.d.	b.d.	b.d.	b.d.	b.d.	b.d.	b.d.	b.d.	b.d.	b.d.	b.d.	b.d.
Lu	b.d.	b.d.	b.d.	0.017	b.d.	0.02	0.014	b.d.	b.d.	b.d.	b.d.	0.014
Hf	0.059	0.063	0.24	0.23	0.23	0.16	2.16	b.d.	b.d.	0.101	0.058	0.77
W	b.d.	b.d.	b.d.	b.d.	b.d.	b.d.	0.141	0.16	b.d.	0.129	b.d.	0.14
Bi	b.d.	b.d.	b.d.	b.d.	b.d.	b.d.	93.66	b.d.	b.d.	b.d.	0.021	46.84
Th	b.d.	0.013	b.d.	0.02	b.d.	0.02	1.65	b.d.	0.049	0.022	0.102	0.37
U	b.d.	b.d.	b.d.	b.d.	b.d.	b.d.	19.89	b.d.	b.d.	b.d.	b.d.	19.89

b.d., below detection limit; data obtained by the LA-ICP-MS method.

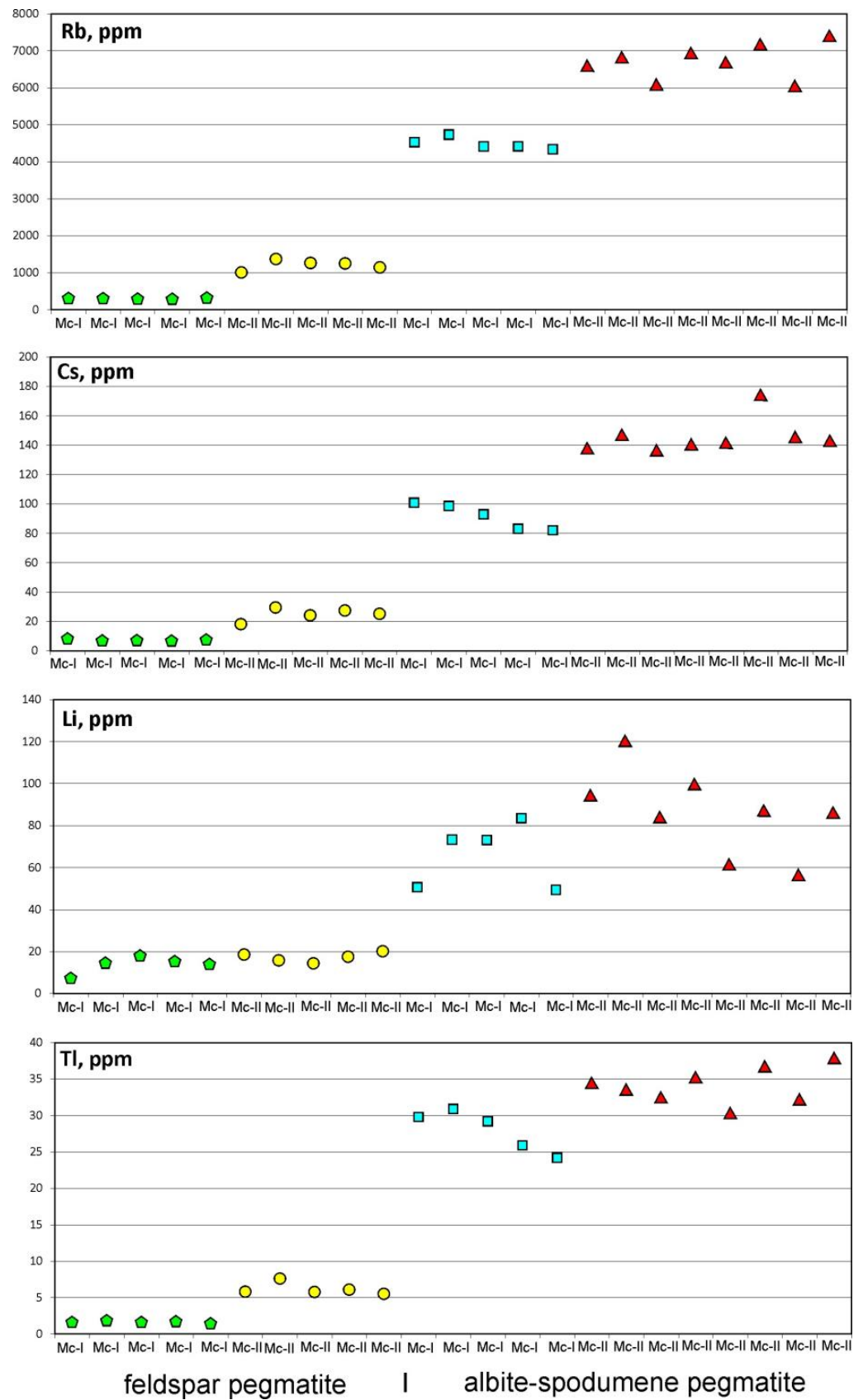


Figure 6. Cont.

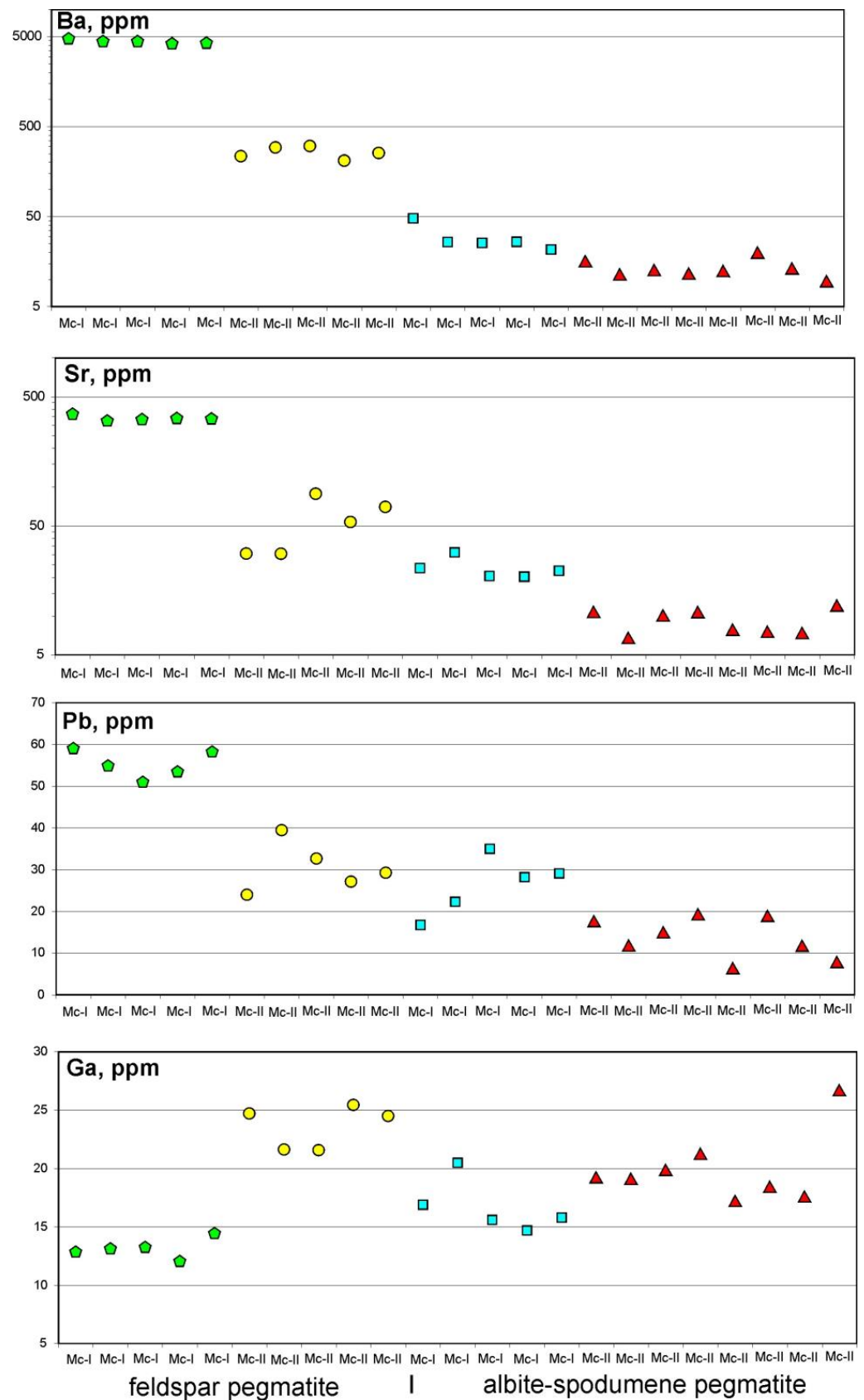


Figure 6. Rb, Cs, Li, Tl, Ba, Sr, Pb, and Ga distributions in early (Mc-I) and late (Mc-II) K-feldspars from feldspar and albite-spodumene pegmatites of the Kolmozero deposit. Albite-spodumene pegmatites: Mc-I (blue squares), Mc-II (red triangles). Feldspar pegmatites: Mc-I (green pentagons), Mc-II (yellow circles).

Chondrite-normalized REE patterns for microcline-II from albite-spodumene pegmatite define an asymmetrical trough broken by a strong negative Eu anomaly (Figure 7). Middle and heavy REE (MREE, HREE) from Gd to Tm have consistent ratios. Overall, the REE concentration in microcline-II is close to chondritic values. On the contrary, the REE concentration in microcline-I from albite-spodumene pegmatite is mainly below the detection limit, except for La having contents 10 times lower than the chondritic values.

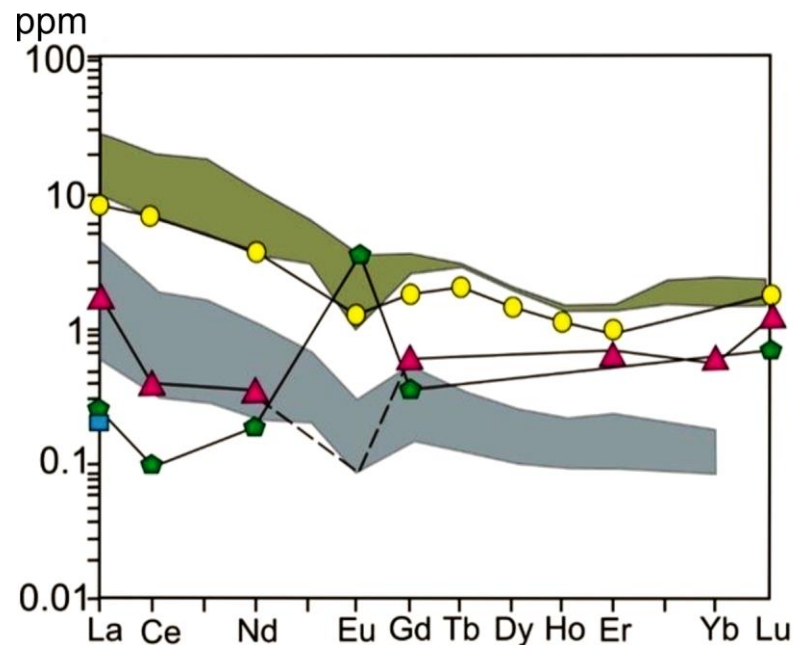


Figure 7. Chondrite-normalized REE distribution in K-feldspar (average data from Tables 2 and 4, same symbols as in Figure 6) and bulk pegmatite (green field is for feldspar pegmatites ($n = 2$), grey field is for albite-spodumene pegmatites ($n = 5$); data after Morozova [15]).

4.3. Geochemistry of K-Feldspar from Feldspar Pegmatites

In general, K-feldspar from feldspar pegmatites has higher Na concentrations than K-feldspar from albite-spodumene pegmatites.

Microcline-I differs from microcline-II in a relatively high content of Sr (340 ppm), Ba (4169 ppm), and Pb (55 ppm), and in low contents of Li (13.7 ppm), Rb (296 ppm), Cs (7 ppm), Tl (1.4 ppm), Ga (13 ppm), Ge (2 ppm), and Mn (1.6 ppm).

In microcline-II, Rb ranges from 1004 to 1261 ppm, while Cs varies from 18 to 29.5 ppm. Lithium contents range from 14.4 to 20 ppm. Concentrations of Tl vary from 5.5 to 7.6 ppm. The content of Mn is very low and varies from 0.69 to 4.9 ppm. K-feldspar contains 259.8 ppm of Ba, 54.7 ppm of Sr and 30.5 ppm of Pb on average. Gadolinium contents range from 21.6 to 25.5 ppm. The average contents of Be (1.8 ppm) and Ta (0.79 ppm) are very low. Niobium is present in concentrations of 0.06 to 15.9 ppm. In general, megacrystic blocky K-feldspar from feldspar pegmatites is depleted in Rb, Cs, Li, Tl, and Mn, though enriched in Sr, Ba, Pb compared to K-feldspars (microcline-I and microcline-II) from albite-spodumene pegmatites.

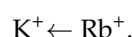
The chondrite-normalized REE patterns for K-feldspars from barren feldspar pegmatite are different for microcline-I and microcline-II. Microcline-II has a slightly increasing slope from LREE to HREE broken by a strong positive Eu anomaly (Figure 7). Microcline-II shows a slightly falling slope from LREE to HREE with a moderate negative Eu anomaly. Overall, REE concentrations in microcline-II are higher (for LREE) or close to (for HREE) chondritic values. REE concentrations in microcline-I are lower than chondritic values, except for Eu.

5. Discussion

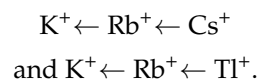
This study utilizes mineral chemical and crystal structure information of K-feldspar to reveal the sequence crystallization of pegmatite of the Kolmozero field. Of particular interest is the comparison of compositions of K-feldspars from feldspar pegmatites and Li-mineralized albite-spodumene pegmatites. The results of this study show significant variations in the content of trace elements in K-feldspars from albite-spodumene pegmatites and feldspar pegmatites. In K-feldspar, the concentration variations of minor elements depend on certain factors, such as isomorphic substitution in the structure of K-feldspar, PT-conditions of crystallization, composition and evolution of pegmatite-forming melt and fluid, mineral associations, textural evolution of pegmatites, etc. [31–33].

5.1. Crystallochemical Control

A significant proportion of minor and trace elements have been incorporated into the crystal structure of K-feldspar. Here, the *T* position is filled with Al^{3+} , Si^{4+} , Ga^{3+} , Fe^{3+} , P^{5+} and Ge^{4+} , and the *M* position is filled with Ca^{2+} , Na^+ , K^+ , Rb^+ , Cs^+ , Li^+ , Sr^{2+} , Ba^{2+} , Tl^+ , Mn^{2+} , Fe^{2+} , Eu^{2+} , and Pb^{2+} [12,28–30,33–37]. Rubidium and K have a similar structure of electron shells, identical valence, and similar ionic radii. Their ionization potentials and electronegativities are identical. The isomorphous incorporation of Rb^+ cation into K-feldspar proceeds according to the scheme:



Cesium has a larger ionic radius, lower electronegativity, and lower ionization potential than K. Consequently, the dispersion of the Cs content in the K-feldspar is much greater than that of Rb. Tl has a slightly higher electronegativity and ionization potential than both K and Rb, and its bonding to oxygen is more covalent. Its ionic radius is virtually equal to that of Rb. The isomorphous incorporation of Cs^+ and Tl^+ cations into K-feldspar follows the schemes:



Ionic radii of Pb and K are similar, but K and Pb significantly differ in their electronegativity and ionization potential. In K-feldspar, the isomorphic replacement of K for Pb is limited. K-feldspar also contains elements that are not present in its crystal structure. In K-feldspar from pegmatites of the Kolmozero pegmatite field, these elements could be due to microinclusions of minerals.

The most important minor elements in the Kolmozero K-feldspar are Rb, Cs, Li, and Tl. In microcline-I and microcline-II, typical impurity elements enter the crystal lattice of K-feldspar in the following order: $\text{Rb} \gg \text{Cs} > \text{Li} > \text{Tl}$. Microcline-II is higher in Rb, Cs, Li, and Tl and lower in Sr, Ba, and Pb compared to microcline-I (Figure 7).

According to V.V. Gordienko [14], the Kolmozero K-feldspar contains 69 % of Rb of the total whole rock amount and 29.6 % is bound by muscovite. K-feldspar contains 45 % of Cs of the total whole rock amount, and 41.9 % is bound by muscovite, and 11.7 % is bound by beryl. It should be noted that the Kolmozero K-feldspar has a higher K/Rb ratio and lower Cs content than K-feldspar from the Tanco zoned pegmatite (Manitoba state [38]) (Figure 8b). However, similar K/Rb ratios (35–15) are observed in K-feldspar from albite-spodumene pegmatites of the Kings Mountain deposit (North Carolina, USA) [33]. The Kolmozero K-feldspar is depleted in REE compared to K-feldspar from pegmatites of the NYF (niobium-yttrium-fluorine) family (cf., e.g., [38]).

However, Ba ($\text{Ba} \gg \text{Sr} > \text{Rb}$) is the dominant minor element in microcline-I from feldspar pegmatites of the Kolmozero pegmatite field. However, in microcline-II, from feldspar pegmatites, minor elements are arranged as follows: $\text{Rb} \gg \text{Ba} > \text{Sr}$. K-feldspars from feldspar pegmatites of the Kolmozero pegmatite field have the same K/Rb ratios and Cs contents as K-feldspar from Lake Osis pegmatitic granite (Manitoba state) (Figure 8b).

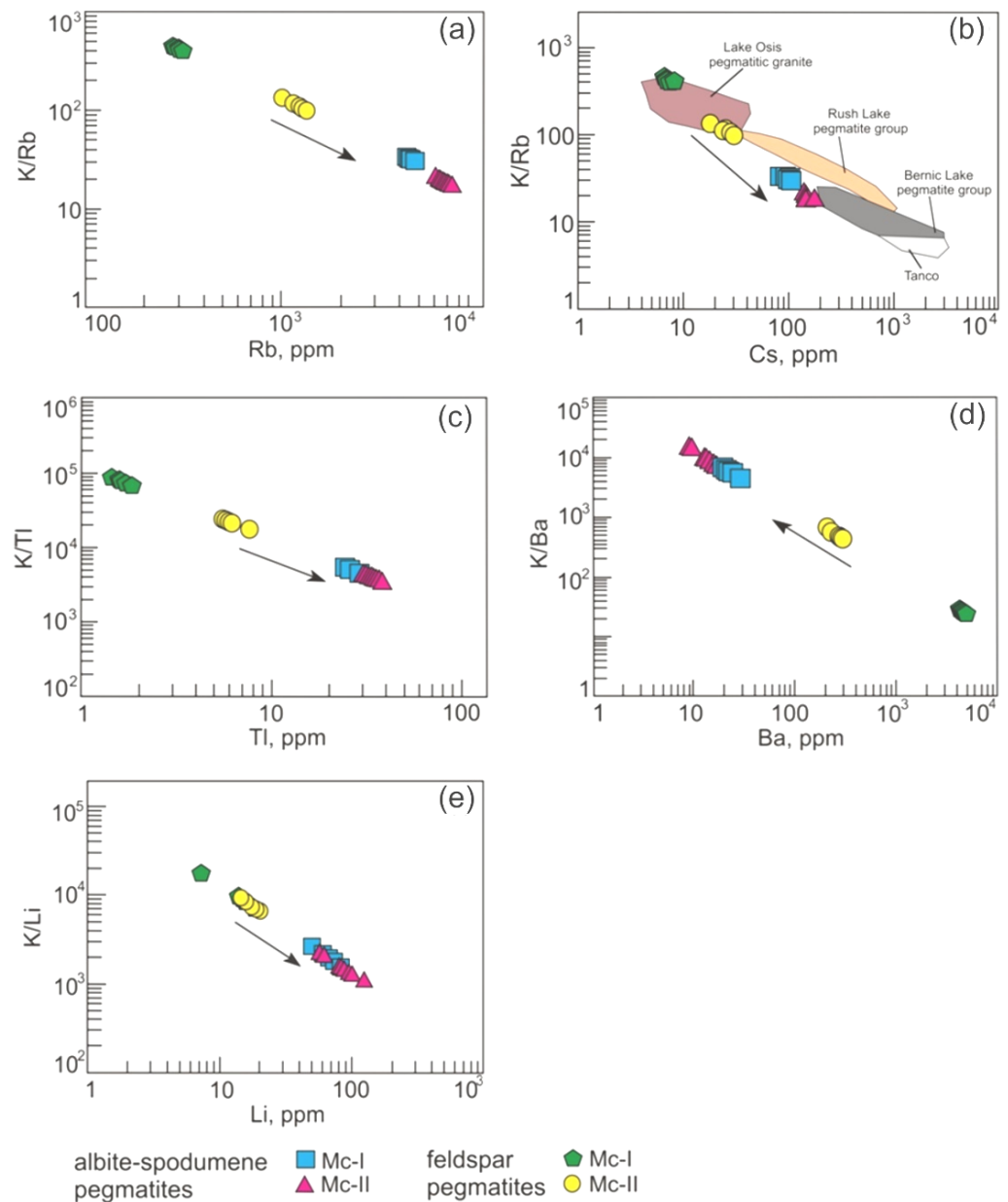


Figure 8. (a) Plots of K/Rb vs. Rb; (b) K/Cs vs. Cs (feldspars from Bernic Lake pegmatite group, Tanco pegmatite, Rush Lake pegmatite group, and Lake Osis pegmatitic granite are from Goad and Černý [39]); (c) K/Tl vs. Tl; (d) K/Ba vs. Ba; (e) K/Li vs. Li. In K-feldspars, K/Ba ratios and the contents of Rb, Cs, Tl, and Li increase, while K/Rb, K/Tl, and K/Li element ratios and the contents of Ba decrease from feldspar pegmatites to albite-spodumene pegmatites. Similar trends are observed from early to late generations of K-feldspar.

In general, the content of Rb, Cs, Li, and Tl, in K-feldspar from pegmatites of the Kolmozero pegmatite field increases, while the content of Ba, Sr, and Pb decreases from feldspar pegmatites to albite-spodumene pegmatites. In K-feldspar, the K/Rb, K/Cs, K/Tl, and K/Li element ratios decrease, while the K/Sr and K/Ba element ratios increase from feldspar pegmatites to albite-spodumene pegmatites (Table 5; Figure 8). In terms of the K/Rb element ratio and Cs content, K-feldspar from pegmatites of the Kolmozero pegmatite field show trends generally akin to K-feldspar in pegmatites of the Winnipeg River region (Manitoba state) (Figure 8b).

Table 5. Ratio of trace elements in K-feldspar. Determined by EMPA and LA-ICP-MS.

Type Pegmatites	Feldspar Pegmatites		Albite-Spodumene Pegmatites	
	Mc-I Average [Range] n = 5	Mc-II Average [Range] n = 5	Mc-I Average [Range] n = 5	Mc-II Average [Range] n = 8
K/Rb	440 [462–415]	111 [134–98]	30 [30–28]	20 [22–18]
K/Cs	18,153 [19,525–15,907]	5478 [7364–4547]	1460 [1618–1311]	912 [976–758]
K/Tl	80,303 [91,329–72,019]	21,952 [24,227–17,628]	4765 [5467–4267]	3896 [4404–3476]
K/Li	10,429 [17,912–7217]	7844 [9248–6640]	2019 [2684–1589]	1619 [2356–1102]
K/Sr	382 [405–352]	2939 [4408–1497]	5758 [6576–4239]	21,988 [72,200–10,906]
K/Ba	30 [27–31]	525 [435–636]	4854 [6165–2752]	10,323 [13,709–8109]
Rb/Ba	0.07 [0.06–0.07]	4.5 [4.1–5.9]	163 [94–201]	525 [359–770]
Rb/Sr	0.87 [0.82–0.93]	22 [14–23]	190 [152–215]	799 [612–3613]

During cooling, feldspars demonstrate subsolidus processes, including ordering of the structure, recrystallization, development of twins, and variations in chemical composition [12,40].

5.2. Evolution of Kolmozero Pegmatite System

In the pegmatite system, fractionation of alkaline and alkaline-earth elements can be caused by (1) fractional crystallization, and (2) hydrothermal processes. The crystal/melt partition coefficient of K is greater than Rb, which is greater than Cs. Residual melts become progressively enriched in Rb and Cs during crystallization. The lower K/Rb, K/Cs ratios and higher Rb and Cs contents of evolved bulk pegmatites and their constituent minerals would then be inherited from the evolved residual melts. The partition coefficients for Ba and Sr are higher than for K, in an increase in K/Ba and K/Sr and lower Ba and Sr contents of residual melts. In contrast, during hydrothermal processes Ba and to a lesser extent Sr tend to accumulate at the latest stages [41,42]. The trends observed in the Kolmozero deposit suggest the following sequence of K-feldspar crystallization (from early to late): microcline-I (feldspar pegmatite) → microcline-II (feldspar pegmatite) ~ / → microcline-I (spodumene pegmatite) → microcline-II (spodumene pegmatite). The K/Rb, K/Cs, and K/Ba ratios are in accordance with this sequence (see Figure 8), confirming the crucial role of fractional crystallization rather than of hydrothermal processes in the evolution of the Kolmozero pegmatite system. The progressive enrichment of highly incompatible LREE in the studied sequence (La/Ndn has values 1.3, 2.2 for microcline-I and microcline-II from feldspar pegmatite, respectively, and 4.8 for microcline-II from albite-spodumene pegmatite) is associated with fractional crystallization. The chondrite-normalized REE patterns for bulk pegmatite are similar to feldspar patterns (Figure 7), assuming that they are the principal hosts for REE in the pegmatites. The average values of La/Ndn are 2.7 and 3.0 in feldspar and albite-spodumene pegmatites, respectively; these also withstand a higher degree of fractionation in albite-spodumene pegmatites.

In decreasing order of significance, trace quantities of Ba, Sr, Pb and Ga occur within the K-feldspars and appear to be other important trace elements in K-feldspar from the Kolmozero pegmatites (Table 5). The Pb content in K-feldspar decreases with the temporal evolution of pegmatites (early to late). This trend is also reported for other pegmatite fields [43], and even for a single pegmatite body [42]. Compared to more incompatible Rb, the Rb/Sr and Rb/Ba (Table 5) ratios increase from feldspar pegmatites to albite-spodumene

pegmatites and from the early K-feldspar to the late one, enhancing the preferential increase of more incompatible elements during fractional crystallization. The concentration of Ga is nearly constant for both pegmatite types and slightly increases from early to late K-feldspar. This is probably not controlled by K-feldspar fractionation and the Ga distribution is either (1) buffered by other phases, or (2) reflects the involvement of the fluid components [6].

Thus, the obtained geochemical data imply that pegmatites of the Kolmozero pegmatite field are cogenetic and were formed during fractional crystallization. Similar trends have also been described for K-feldspars from granite-pegmatite systems in other regions [3,6,7,11,35,42–48]. The commonly adopted spatial model comprises (1) an area of barren pegmatites followed by pegmatites with the Be-mineralization in the direct vicinity of parental fertile granites; next, (2) an area of pegmatites rich in Be, Nb, and Ta followed by an area of pegmatites with increased concentrations of Li, Be, Nb, and Ta; (3) an area of pegmatites with increased concentrations of Cs, Li, Be, Nb, and Ta is the most remote [39,49]. The granite source for the Kolmozero albite-spodumene pegmatites has not been identified and we cannot exclude the formation of pegmatites by anatexis of host amphibolites and gneisses as proposed for a number of pegmatitic fields (e.g., in South Norway [50], and elsewhere [9,13,51–59]). However, our data suggest that a parental fertile granite of the Kolmozero pegmatites may be unexposed and occur at depth, below the feldspar pegmatites. Many other pegmatite fields across the world also feature the most primitive pegmatites in a proximal position with respect to the presumed source-area of pegmatite forming melts [6,7,39,49,59].

5.3. Distinction between Different Mineralization Types

The mineral chemistry of K-feldspars including element ratios indicate geochemical specialization of different pegmatites at Kolmozero. Our data show that K-feldspars from feldspar pegmatites with Be-mineralization and K-feldspars from albite-spodumene pegmatites with Be-Ta-Nb-Li-mineralization differ in Rb, Cs, Li, and Tl contents (up to one order higher in the albite-spodumene type) and in the corresponding element ratios (Figure 8, Tables 2, 4 and 5). These data can be used for mineral exploration for lithium in pegmatite deposits.

According to our data, megacrystic (blocky) K-feldspar from both albite-spodumene pegmatites and feldspar pegmatites is classified as a maximum microcline with high ordering. According to Černý [3], the megacrystic (blocky) microcline from fertile granite pegmatites is often ordered up to the maximum.

6. Conclusions

K-feldspar is one of the main rock-forming minerals in pegmatites of the Kolmozero field at the Kola peninsula, Russia. Megacrystic blocky K-feldspar occurs as two generations, microcline-I (Mc-I) and microcline-II (Mc-II), in primitive feldspar pegmatites and evolved albite-spodumene pegmatites. The results of the chemical studies of these microclines can be summarized as follows:

(1) Rubidium, Cs, Li and Tl are the most common impurity elements in K-feldspar and replace K in its crystal lattice. Microcline-II differs from microcline-I by having a relatively high content of Rb (6519 ppm), Cs (146 ppm), Li (86 ppm), Tl (34 ppm), and low contents of Ba (13 ppm), Sr (8 ppm), Pb (14 ppm), and an albite component (Ab_{03}).

(2) K-feldspar from feldspar pegmatites within the Kolmozero pegmatite field differs from those from the Kolmozero Li deposit, being characterized by low contents of Rb, Cs, Li, and Tl, as well as comparatively higher concentrations of Sr, Ba, and Pb.

(3) In K-feldspars, K/Ba, K/Sr, Rb/Ba, and Rb/Sr element ratios increase, while K/Rb, K/Cs, K/Tl, and K/Li element ratios decrease from feldspar pegmatites to albite-spodumene pegmatites. These trends indicate the possible genetic link between feldspar pegmatites and albite-spodumene pegmatites and that the obtained trace element variability is due to fractional crystallization. The contents of Rb, Cs, Li, and Tl and their indicator ratios can be used to determine the temporal evolution of certain pegmatite systems and

as an effective tool in mineral exploration for lithium, because K-feldspar is ubiquitous in various types of pegmatites.

Author Contributions: Conceptualization, L.M.; investigation, L.M., D.Z., A.B. and E.S.; resources, L.M.; writing—original draft preparation, L.M., D.Z., P.S. and E.S.; writing—review and editing, L.M., D.Z. and E.S.; project administration, L.M. and D.Z.; formal analysis, A.B. and E.S. All authors have read and agreed to the published version of the manuscript.

Funding: The research has been carried out in the framework of the Russian Science Foundation. Grant № 22-17-20002, <https://rscf.ru/project/22-17-20002/> (accessed on 25 March 2022).

Data Availability Statement: Not applicable.

Acknowledgments: The authors express their gratitude to E.L. Kunakkuzin, E.S. Borisenko, A.N. Ivanov and I.A. Koval (GI KSC RAS) for their assistance during field work. We thank the anonymous reviewers and the Academic Editors for very helpful comments on the manuscript.

Conflicts of Interest: The authors declare no conflict of interest.

References

1. Kesler, S.E.; Gruber, P.W.; Medina, P.A.; Keoleian, G.A.; Everson, M.P.; Wallington, T.J. Global lithium resources: Relative importance of pegmatite, brine and other deposits. *Ore Geol. Rev.* **2012**, *48*, 55–69. [\[CrossRef\]](#)
2. Howell, R.J.; Lagos, L.; Hoyos, C.R.D.L.; Declercq, J. Classification and Characteristics of Natural Lithium Resources. *Elements* **2020**, *16*, 259–264. [\[CrossRef\]](#)
3. Černý, P. Evolution of Feldspars in Granitic Pegmatites. In *Feldspars and Their Reactions*; Parsons, I., Ed.; NATO ASI Series 421; NATO: Brussels, Belgium, 1994; pp. 501–540. [\[CrossRef\]](#)
4. Neiva, A.M.R. Distribution of trace elements in feldspars of granitic aplites and pegmatites from Alijó-Sanfins, northern Portugal. *Miner. Mag.* **1995**, *59*, 35–45. [\[CrossRef\]](#)
5. Neiva, A. Micas, feldspars and columbite-tantalite minerals from the zoned granitic lepidolite-subtype pegmatite at Namivo, Alto Ligonha, Mozambique. *Eur. J. Miner.* **2013**, *25*, 967–985. [\[CrossRef\]](#)
6. Larsen, R.B. The Distribution of Rare-Earth Elements in K-Feldspar as an Indicator of Petrogenetic Processes in Granitic Pegmatites: Examples from Two Pegmatite Fields in Southern Norway. *Can. Miner.* **2002**, *40*, 137–152. [\[CrossRef\]](#)
7. Alfonso, P.; Melgarejo, J.C.; Yusta, I.; Velasco, F. Geochemistry of Feldspars and Muscovite in Granitic Pegmatite from the Cap De Creus Field, Catalonia, Spain. *Can. Miner.* **2003**, *41*, 103–116. [\[CrossRef\]](#)
8. Oyarzabal, J.; Perino, E.; Galliski, M. Geochemistry of K-feldspar and Muscovite in Rare-element Pegmatites and Granites from the Totoral Pegmatite Field, San Luis, Argentina. *Resour. Geol.* **2009**, *59*, 315–329. [\[CrossRef\]](#)
9. London, D.; Morgan, V.G.B. The Pegmatite Puzzle. *Elements* **2012**, *8*, 263–268. [\[CrossRef\]](#)
10. Marchal, K.L.; Simmons, W.; Falster, A.U.; Webber, K.L.; Roda-Robles, E.; Bo, F.D.; Hatert, F.; Baijot, M. Geochemistry, Mineralogy, and Evolution of Li-Al Micas and Feldspars from the Mount Mica Pegmatite, Maine, USA. *Can. Miner.* **2014**, *52*, 221–233. [\[CrossRef\]](#)
11. Hulsbosch, N.; Hertogen, J.; Dewaele, S.; André, L.; Muchez, P. Alkali metal and rare earth element evolution of rock-forming minerals from the Gatumba area pegmatites (Rwanda): Quantitative assessment of crystal-melt fractionation in the regional zonation of pegmatite groups. *Geochim. Cosmochim. Acta* **2014**, *132*, 349–374. [\[CrossRef\]](#)
12. Sánchez-Muñoz, L.; García-Guinea, J.; Zagorsky, V.Y.; Juwono, T.; Modreski, P.J.; Cremades, A.; Van Tendeloo, G.; De Moura, O.J.M. The Evolution of Twin Patterns in Perthitic K-Feldspar from Granitic Pegmatites. *Can. Miner.* **2012**, *50*, 989–1024. [\[CrossRef\]](#)
13. Thomas, R.; Davidson, P.; Beurlen, H. The competing models for the origin and internal evolution of granitic pegmatites in the light of melt and fluid inclusion research. *Miner. Pet.* **2012**, *106*, 55–73. [\[CrossRef\]](#)
14. Gordienko, V.V. *Mineralogy, Geochemistry and Genesis of Spodumene Pegmatites*; Nedra: Leningrad, Russia, 1970.
15. Morozova, L.N. Geological Institute KSC RAS Lithium Kolmozero deposit of rare metal pegmatites: New data on rare element composition (Kola Peninsula). *LITOSFERA* **2018**, *18*, 82–98. [\[CrossRef\]](#)
16. Daly, J.S.; Balagansky, V.V.; Timmerman, M.J.; Whitehouse, M.J. The Lapland-Kola orogen: Palaeoproterozoic Collision and Accretion of the Northern Fennoscandian Lithosphere. In *European Lithosphere Dynamics*; Gee, D.G., Spephenson, R.A., Eds.; Memoir 32; Geological Society: London, UK, 2006; pp. 579–598. [\[CrossRef\]](#)
17. Timmerman, M.J.; Daly, J. Sm-Nd evidence for late Archaean crust formation in the Lapland-Kola Mobile Belt, Kola Peninsula, Russia and Norway. *Precambrian Res.* **1995**, *72*, 97–107. [\[CrossRef\]](#)
18. Rundqvist, D.V.; Mitrofanov, F.P. (Eds.) *Precambrian Geology of the USSR*; Elsevier Sci.: Amsterdam, The Netherlands, 1993.
19. Mints, M.V. Paleoproterozoic and Mesoproterozoic microcontinents. In *East European Craton: Early Precambrian History and 3D Models of Deep Crustal Structure*; Condie, K., Harvey, F.E., Eds.; Spec. Paper 510; Geological Society of America: Boulder, CO, USA, 2015; pp. 19–32. [\[CrossRef\]](#)
20. Glebovitsky, V.A. (Ed.) *Early Precambrian of the Baltic Shield*; Nauka: St. Petersburg, Russia, 2005.
21. Lahtinen, R.; Huhma, H. A revised geodynamic model for the Lapland-Kola Orogen. *Precambrian Res.* **2019**, *330*, 1–19. [\[CrossRef\]](#)

22. Kudryashov, N.M.; Petrovsky, M.N.; Mokrushin, A.V.; Elizarov, D.V. Neoproterozoic sanukitoid magmatism in the Kola region: Geological, petrochemical, geochronological, and isotopic-geochemical data. *Petrology* **2013**, *21*, 351–374. [[CrossRef](#)]
23. Vrevsky, A.B.; Lvov, A.P. Isotopic age and heterogeneous sources of gabbro—anorthosites from the Patchemvarek massif, Kola Peninsula. *Dokl. Earth Sci.* **2016**, *469*, 716–721. [[CrossRef](#)]
24. Morozova, L.N.; Bayanova, T.B.; Bazai, A.V.; Lyalina, L.M.; Serov, P.A.; Borisenko, E.S.; Kunakkuzin, E.L. Rare metal pegmatites of the Kolmozerskoe lithium deposits of the Arctic region, the Baltic shield: New geochronological data. *Vestnik KNC RAS* **2017**, *9*, 43–52. (In Russian)
25. Morozova, L.N.; Sokolova, E.N.; Smirnov, S.Z.; Balagansky, V.V.; Bazai, A.V. Spodumene from rare-metal pegmatites of the Kolmozero lithium world-class deposit on the Fennoscandian shield: Trace elements and crystal-rich fluid inclusions. *Miner. Mag.* **2021**, *85*, 149–160. [[CrossRef](#)]
26. Černý, P. Rare-element granitic pegmatites. Part I: Anatomy and internal evolution of pegmatitic deposits. *Geosci. Can.* **1991**, *18*, 49–67.
27. Lafuente, B.; Downs, R.T.; Yang, H.; Stone, N. 1. The Power of Databases: The RRUFF Project. In *Highlights in Mineralogical Crystallography*; Armbruster, T., Danisi, R.M., Eds.; De Gruyter: Berlin, Germany, 2016; ISBN 9783110417104.
28. Smith, J.; Brown, W.L. *Feldspar Minerals. 1. Crystal Structures, Physical, Chemical and Micro-Textural Properties*, 2nd ed.; Springer: New York, NY, USA, 1988. [[CrossRef](#)]
29. Deer, W.A.; Howie, R.A.; Zussman, J. *Rock Forming Minerals. 2A. Single-Chain Silicates*, 2nd ed.; Longman: London, UK, 1978. [[CrossRef](#)]
30. Bulakh, A.G.; Zolotaryov, A.A.; Krivovichev, V.G. *Structure, Isomorphism, Formulas, and Classification of Minerals*; SPbU Publishing: St. Petersburg, Russia, 2014.
31. London, D.; Stein, H.J.; Hannah, J.L. Internal differentiation of rare-element pegmatites; A synthesis of recent research. *Geol. Soc. America, Spec. Paper* **1990**, *246*, 35–50. [[CrossRef](#)]
32. London, D. The application of experimental petrology to the genesis and crystallization of the granitic pegmatites. *Can. Min.* **1992**, *30*, 499–540.
33. Černý, P.; Meintzer, R.E.; Anderson, A.J. Extreme fractionation in rare-element granitic pegmatites: Selected examples of data and mechanisms. *Can. Mineral.* **1985**, *23*, 381–421.
34. Goldschmidt, V.M. *Geochemistry*; Clarendon Press: Oxford, UK, 1958.
35. Gordienko, V.V. *Granite Pegmatites*; SPbU Publishing: St. Petersburg, Russia, 1996.
36. Sánchez-Muñoz, L.; Müller, A.; Andrés, S.L.; Martin, R.F.; Modreski, P.J.; de Moura, O.J. The P–Fe diagram for K-feldspars: A preliminary approach in the discrimination of pegmatites. *Lithos* **2017**, *272–273*, 116–127. [[CrossRef](#)]
37. Bambauer, H.U.; Krause, C. TEM-investigation of the sanidine/microcline transition across metamorphic zones: The K-feldspar varieties. *Eur. J. Miner.* **1989**, *1*, 47–58. [[CrossRef](#)]
38. Goad, B.E.; Černý, P. Peraluminous pegmatitic granites and their pegmatite aureoles in the Winnipeg River district, southeastern Manitoba. *Can. Min.* **1981**, *19*, 177–194.
39. London, D. *Pegmatites*; The Canadian Mineralogist. Special Publication 10; Mineralogical Association of Canada: Quebec, QC, Canada, 2008.
40. Fischer, K.; Puchelt, H. *Handbook of Geochemistry, Chapter 56 Barium*; Wedepohl, K.H., Ed.; Springer: New York, NY, USA, 1972.
41. Wedepohl, K.H. *Strontium: Abundance in Common Igneous Rock Types*; Springer: Cham, Switzerland, 1978.
42. Kontak, D.J.; Martin, R.F. Alkali feldspar in the peraluminous South Mountain batholith, Nova Scotia: Trace element data. *Can. Mineral.* **1997**, *35*, 959–977.
43. Černý, P.; Trueman, D.L.; Ziehkle, D.V.; Goad, B.E.; Paul, B.J. *The Cat Lake-Winnipeg River and the Wekusko Lake Pegmatite Fields, Manitoba*; Manitoba Department of Energy and Mines, Mineral Resources Division: Winnipeg, MB, Canada, 1981; p. ER80-1.
44. Černý, P.; Teertstra, D.K.; Chapman, R.; Selwal, J.B.; Hawthorne, F.C.; Ferreira, K.; Chackowsky, L.E.; Wang, X.-J.; Meintzer, R.E. Extreme fractionation and deformation of the leucogranite—Pegmatite suite at Red Cross Lake, Manitoba, Canada. IV. Mineralogy. *Can. Min.* **2012**, *50*, 1839–1875. [[CrossRef](#)]
45. Breaks, F.W.; Selway, J.B.; Tindle, A.C. Fertile Peraluminous Granites and Related Rare-Element Pegmatites, Superior Province of Ontario. In *Rare-Element Geochemistry and Mineral Deposits*; Linnen, R.L., Sampson, I.M., Eds.; The Geological Association of Canada: St. Catharines, Canada, 2005; pp. 87–125.
46. Selway, J.B.; Breaks, F.W.; Tindle, A.G. A Review of Rare-Element (Li-Cs-Ta) Pegmatite Exploration Techniques for the Superior Province, Canada, and Large Worldwide Tantalum Deposits. *Explor. Min. Geol.* **2005**, *14*, 1–30. [[CrossRef](#)]
47. Brown, J.A.; Martins, T.; Černý, P. The Tanco Pegmatite At Bernic Lake, Manitoba. XVII. Mineralogy and Geochemistry of Alkali Feldspars. *Can. Miner.* **2017**, *55*, 483–500. [[CrossRef](#)]
48. Tang, Y.; Wang, H.; Zhang, H.; Lv, Z.-H. K-feldspar composition as an exploration tool for pegmatite-type rare metal deposits in Altay, NW China. *J. Geochem. Explor.* **2018**, *185*, 130–138. [[CrossRef](#)]
49. Černý, P. Exploration Strategy and Methods for Pegmatite Deposits of Tantalum. In *Lanthanides, Tantalum and Niobium*; Möller, P., Černý, P., Saupé, F., Eds.; Springer: Berlin/Heidelberg, Germany, 1989; pp. 274–302. [[CrossRef](#)]
50. Müller, A.; Romer, R.L.; Pedersen, R.-B. The Sveconorwegian Pegmatite Province—Thousands of Pegmatites Without Parental Granites. *Can. Miner.* **2017**, *55*, 283–315. [[CrossRef](#)]

51. Fuchsloch, W.C.; Nex, P.A.; Kinnaird, J.A. Classification, mineralogical and geochemical variations in pegmatites of the Cape Cross-Uis pegmatite belt, Namibia. *Lithos* **2018**, *296*, 79–95. [[CrossRef](#)]
52. Simmons, W.; Falster, A.; Webber, K.; Roda-Robles, E.; Boudreaux, A.P.; Grassi, L.R.; Freeman, G. Bulk Composition of Mt. Mica Pegmatite, Maine, USA: Implications for the Origin of An Lct Type Pegmatite By Anatexis. *Can. Miner.* **2016**, *54*, 1053–1070. [[CrossRef](#)]
53. Simmons, W.B.; Foord, E.E.; Falster, A.U. *Anatectic Origin of Granitic Pegmatites, Western Maine, USA, GAC-MAC Annual Meeting—Abstracts with Programs*; University of Manitoba: Winnipeg, MB, USA, 1996.
54. Turlin, F.; Vanderhaeghe, O.; Gervais, F.; André-Mayer, A.S.; Moukhsil, A.; Zeh, A.; Solgadi, F.; I.P.T.N. Petrogenesis of LREE-rich pegmatitic granite dykes in the central Grenville Province by partial melting of Paleoproterozoic-Archean metasedimentary rocks: Evidence from zircon U-Pb-Hf-O isotope and trace element analyses. *Precambrian Res.* **2019**, *327*, 327–360. [[CrossRef](#)]
55. Webber, K.; Simmons, W.B.; Falster, A.U.; Hanson, S.L. Anatectic Pegmatites of the Oxford County Pegmatite Field, Maine, USA. In Proceedings of the 9th International Symposium on Granitic Pegmatites, Pala, CA, USA, 30 September 2019; Wise, M., Brown, C., Simmons, W.B., Roda-Robles, E., Webber, K., Eds.; pp. 87–90.
56. Wise, M.A.; Müller, A.; Simmons, W.B. A proposed new mineralogical classification system for granitic pegmatites. *Can. Miner.* **2022**, *60*, 229–248. [[CrossRef](#)]
57. Konzett, J.; Schneider, T.; Nedyalkova, L.; Hauzenberger, C.; Melcher, F.; Gerdes, A.; Whitehouse, M. Anatectic Granitic Pegmatites from the Eastern Alps: A Case of Variable Rare-Metal Enrichment During High-Grade Regional Metamorphism—I: Mineral Assemblages, Geochemical Characteristics, and Emplacement Ages. *Can. Miner.* **2018**, *56*, 555–602. [[CrossRef](#)]
58. Schuster, R.; Ilickovic, T.; Mali, H.; Huet, B.; Schedl, A. Permian Pegmatites and Spodumene Pegmatites in the Alps: Formation During Regional Scale High Temperature/Low Pressure Metamorphism. In Proceedings of the 8th International Symposium on Granitic Pegmatites. NGF Abstracts and Proceedings, Kristiansand, Norway, 19 June 2017; Müller, A., Rosing-Schow, N., Eds.; pp. 122–125.
59. Shearer, C.K.; Papike, J.J.; Jolliff, B.L. Petrogenetic links among granites and pegmatites in the Harney Peak rare-element granite-pegmatite system, Black Hills, South Dakota. *Can. Min.* **1992**, *30*, 785–809.